Article

Cell Metabolism

Brown Adipose Tissue Controls Skeletal Muscle Function via the Secretion of Myostatin

Graphical Abstract

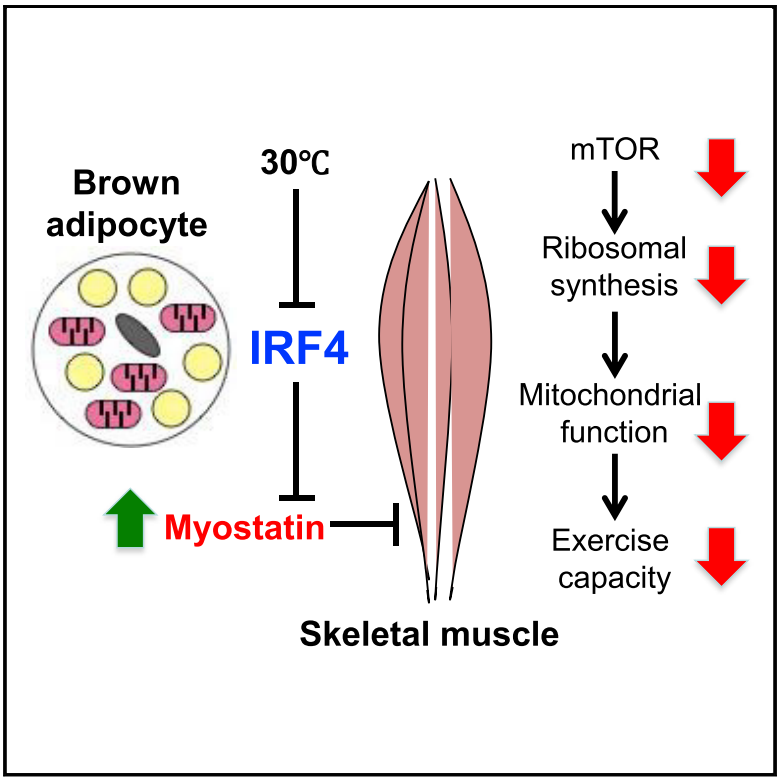

Authors

Xingxing Kong, Ting Yao, Peng Zhou, ..., Bruce M. Spiegelman, Tiemin Liu, Evan D. Rosen

Correspondence

xingxingkong@mednet.ucla.edu (X.K.), tiemin_liu@fudan.edu.cn (T.L.), erosen@bidmc.harvard.edu (E.D.R.)

In Brief

Skeletal muscle and brown adipose tissue (BAT) are functionally interlinked. Kong et al. report on the intriguing role of the transcription factor IRF4 in BAT to mediate BAT-muscle crosstalk through the muscle function inhibitor, myostatin. Thermoneutrality or loss of IRF4 results in elevated serum myostatin levels and decreased exercise capacity.

Highlights

- Loss of IRF4 in BAT causes decreased exercise capacity and a selective myopathy
- IRF4 represses myogenic genes in BAT, including the myokine myostatin
- Neutralizing serum myostatin rescues the ability of BATI4KO mice to exercise normally
- Warming reduces IRF4 in BAT, causing myopathy that is reversed by removal of BAT

Kong et al., 2018, Cell Metabolism *28*, 631–643
October 2, 2018
https://doi.org/10.1016/j.cmet.2018.07.004

CellPress

Cell Metabolism
Article

Brown Adipose Tissue Controls Skeletal Muscle Function via the Secretion of Myostatin

Xingxing Kong,[1,2,8,*] Ting Yao,[2,8] Peng Zhou,[1] Lawrence Kazak,[6] Danielle Tenen,[1] Anna Lyubetskaya,[1] Brian A. Dawes,[1] Linus Tsai,[1] Barbara B. Kahn,[1] Bruce M. Spiegelman,[6] Tiemin Liu,[3,4,5,*] and Evan D. Rosen[1,7,9,*]
[1]Division of Endocrinology, Beth Israel Deaconess Medical Center, Harvard Medical School, Boston, MA 02215, USA
[2]Division of Pediatric Endocrinology, Department of Pediatrics, UCLA Children's Discovery and Innovation Institute, David Geffen School of Medicine at UCLA, Los Angeles, CA 90095, USA
[3]Department of Endocrinology and Metabolism, State Key Laboratory of Genetic Engineering, School of Life Sciences, Zhongshan Hospital, Fudan University, Shanghai 200032, PR China
[4]Institute of Metabolism and Integrative Biology, Collaborative Innovation Center for Genetics and Development, Fudan University, Shanghai 200032, PR China
[5]Key Laboratory of Rare Metabolic Diseases, Nanjing Medical University, 101 Longmian Avenue, Jiangning District, Nanjing 211166, PR China
[6]Dana-Farber Cancer Institute, Harvard Medical School, Boston, MA 02215, USA
[7]Broad Institute, Cambridge, MA 02142, USA
[8]These authors contributed equally
[9]Lead Contact
*Correspondence: xingxingkong@mednet.ucla.edu (X.K.), tiemin_liu@fudan.edu.cn (T.L.), erosen@bidmc.harvard.edu (E.D.R.)
https://doi.org/10.1016/j.cmet.2018.07.004

SUMMARY

Skeletal muscle and brown adipose tissue (BAT) are functionally linked, as exercise increases browning via secretion of myokines. It is unknown whether BAT affects muscle function. Here, we find that loss of the transcription factor IRF4 in BAT (BATI4KO) reduces exercise capacity, mitochondrial function, ribosomal protein synthesis, and mTOR signaling in muscle and causes tubular aggregate formation. Loss of IRF4 induces myogenic gene expression in BAT, including the secreted factor myostatin, a known inhibitor of muscle function. Reducing myostatin via neutralizing antibodies or soluble receptor rescues the exercise capacity of BATI4KO mice. In addition, overexpression of IRF4 in brown adipocytes reduces serum myostatin and increases exercise capacity in muscle. Finally, mice housed at thermoneutrality have reduced IRF4 in BAT, lower exercise capacity, and elevated serum myostatin; these abnormalities are corrected by excising BAT. Collectively, our data point to an unsuspected level of BAT-muscle crosstalk driven by IRF4 and myostatin.

INTRODUCTION

Mammalian brown adipose tissue (BAT) is made up of specialized adipocytes that express uncoupling protein 1 (UCP1), which dissipates the mitochondrial proton gradient, forcing increased flux through the electron transport chain and subsequent heat generation. BAT activation, either by cold exposure or through the actions of β-adrenergic agonists, is associated with reduced body weight and improved glucose and lipid homeostasis in rodents and humans (Kajimura et al., 2015; Schrauwen and van Marken Lichtenbelt, 2016; Vosselman et al., 2013). These actions of BAT on systemic physiology are believed to be cell autonomous, with increased UCP1 expression leading to enhanced substrate consumption and thermogenesis. Additional UCP1-independent thermogenic pathways have recently been described in BAT, but these are also cell autonomous in nature (Ikeda et al., 2017; Kazak et al., 2015, 2017).

Conversely, most of the actions of white adipose tissue on systemic physiology are believed to be mediated by the release of adipokines: small molecules, lipids, and proteins secreted by adipocytes that play an important role on appetite, satiety, insulin action, blood pressure, coagulation, and other homeostatic processes (Rosen and Spiegelman, 2014). Few examples of such factors have been shown to be involved in BAT-related biology, although this may be beginning to change. For example, neuregulin 4, is released from brown adipocytes and plays a role in regulating hepatic lipogenesis (Wang et al., 2014). It is likely that many such "BATokines" remain to be discovered.

We originally identified the transcription factor IRF4 as a regulator of adipogenesis after a DNase hypersensitivity screen revealed an interferon-stimulated response element as an over-represented motif in chromatin regions that become progressively accessible during differentiation (Eguchi et al., 2008). Subsequent work showed that IRF4 is strongly induced by fasting in adipocytes, upon which it simultaneously induces the expression of the enzymatic machinery of lipolysis and represses the corresponding genes that promote lipogenesis (Eguchi et al., 2011). More recently, IRF4 was identified as the transcriptional partner of the co-factor PGC-1α and a critical regulator of mitochondrial biogenesis and thermogenesis in BAT. Mice lacking IRF4 in BAT (BATI4KO) are sensitive to cold exposure and have increased adiposity and insulin resistance on a high-fat diet, while mice overexpressing IRF4 in BAT (BATI4OE) have the opposite phenotype (Kong et al., 2014).

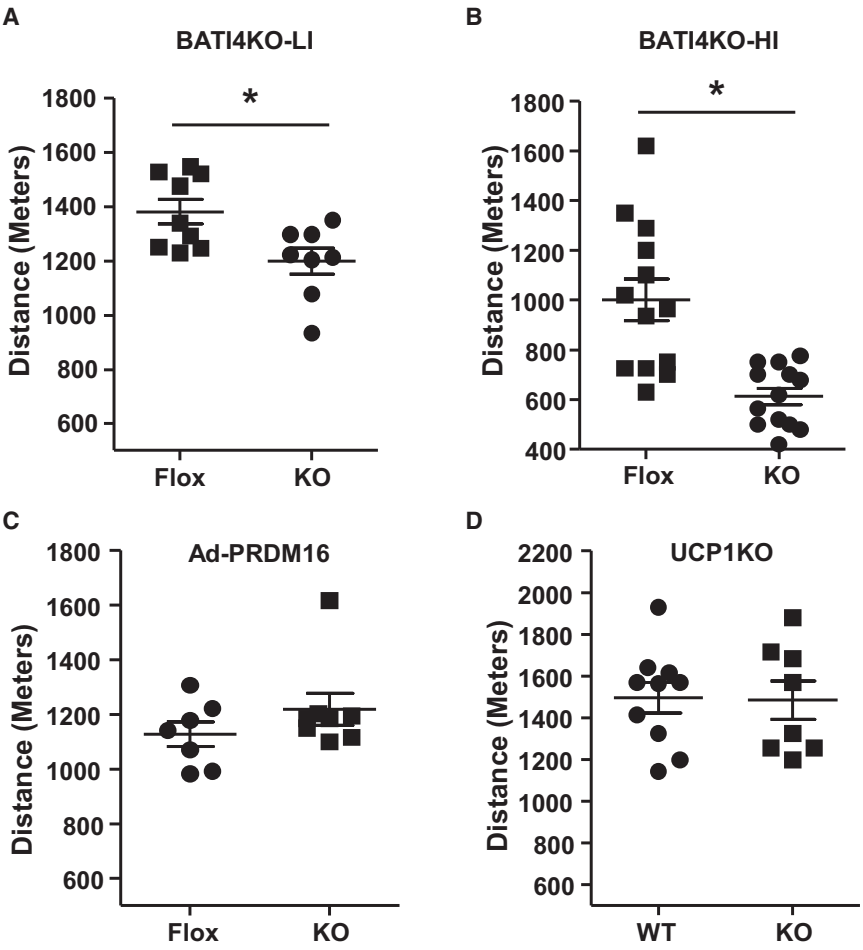

Figure 1. Mice Lacking IRF4 in BAT Have Reduced Exercise Capacity

(A–D) BATI4KO mice showed lower exercise capacity with both a low-intensity (LI) (A) and high-intensity (HI) (B) regimen. The low-intensity exercise regimen was also performed in adipose-specific PRDM16 KO (C) and UCP1KO male mice (D). Results are expressed as means ± SEM (*$p < 0.05$ versus Flox mice).

The BATI4KO and BATI4OE are thus excellent models of deficient and hyperefficient BAT function, generally.

One of the many features of brown fat biology that have gained attention recently is the propensity for exercise to promote browning of white adipose tissue, inducing the formation of thermogenic beige adipocytes with many of the same attributes as interscapular brown fat. Although it is still unclear what purpose this serves in the exercising animal, it is well understood that this occurs through the elaboration of myokines such as irisin/FNDC5, Metrnl, and β-aminoisobutyric acid (Bostrom et al., 2012; Rao et al., 2014; Roberts et al., 2014). Intrigued by these data, we asked whether the skeletal muscle → BAT axis could also communicate in the reverse direction; that is, could skeletal muscle activity be under control of factors from BAT?

RESULTS

Mice Lacking IRF4 in BAT Have Reduced Exercise Capacity

Male, chow-fed BATI4KO mice subjected to a low-intensity treadmill regimen demonstrated diminished exercise capacity by 14% (Figures 1A, S1A, and S1B). Similar results were noted using a high-intensity regimen (38% decreased), as well as free wheel running (Figures 1B and S1C–S1E). Grip strength, however, was unaffected (Figure S1F). These mice have targeted ablation of IRF4 in both interscapular BAT and beige adipocytes, which exist within white depots. Although these mice have greater adiposity than control littermates on a high-fat diet (Kong et al., 2014), there is no difference in body weight, glucose tolerance, or insulin tolerance in chow-fed mice (Figures S1G–S1I). To distinguish which type of thermogenic adipocyte accounts for this effect on running ability we studied adipose-specific Prdm16-deficient mice, which have normal interscapular BAT but are deficient in beige adipocytes (Cohen et al., 2014). These mice exercise normally, suggesting that beige adipocytes are not major drivers of the effect on skeletal muscle (Figure 1C). We also tested mice lacking UCP1 to determine if the thermogenic actions of BAT are required for the effect to take place, but, again, we saw no difference in exercise capacity in this model (Figure 1D). Importantly, we confirmed that our strategy for deleting IRF4 in BAT was not targeting *Irf4* in muscle inappropriately (Figure S1J).

Mice Lacking IRF4 in BAT Have Abnormalities of White Vastus Muscle

The skeletal muscles of BATI4KO mice appear grossly normal, with a normal distribution of type I and type II fibers (Figure S2A). There were, however, signs of myopathy in at least some muscles. Specifically, in the white vastus lateralis we noted nuclear relocation from the periphery to the center of the myofibers after running (Figure 2A), a hallmark of dysfunctional muscle with or without degeneration/regeneration (Roman and Gomes, 2017). This was not seen in control mice, or in the soleus of BATI4KO mice (Figure S2B). Even more strikingly, electron microscopy revealed the presence of tubular aggregates within the white vastus of BATI4KO mice (Figure 2B), a pathological change associated with a variety of myotonic disorders found almost exclusively in type II myocytes (Agbulut et al., 2000; Morgan-Hughes, 1998). Tubular aggregates are believed to derive from expansion of the sarcoplasmic reticulum (SR) (Funk et al., 2013); consistent with this we found greatly enhanced expression of the gene encoding the SR protein Atp2a2 (also called SERCA2) in affected muscles (Figure 2C). We did not

detect significant fibrosis in the vastus of either control or BATI4KO mice (Figure S2C), nor was fiber diameter different (Figure S2D).

To ascertain whether reduced running ability was associated with a metabolic defect in affected muscles, we extracted mitochondria from the vastus lateralis of BATI4KO and control mice and measured the oxygen consumption rate (OCR). Basal (state 4) and ADP-stimulated respiration were unaltered; however, maximal OCR was much lower in the mitochondria from BATI4KO mice compared with control mice (Figure 2D). Given that ADP-stimulated respiration is likely the more significant parameter in the context of exercise, these data may not fully explain the exercise-intolerant phenotype. However, we did note reduced mtDNA content and electron transport protein expression in purified vastus mitochondria (Figures 2E and 2F), without any changes in the soleus (Figures S2E and S2F). We anticipated that these alterations in mitochondrial protein expression would reflect reduced mRNA expression of these genes, but this was not the case. RNA sequencing (RNA-seq) and qPCR analysis from white vastus of BATI4KO mice revealed diminished expression of a few mitochondrial genes (e.g., *Cox4* and *Ucp3*), but the majority of mitochondrial proteins displayed unchanged levels of mRNA (Figures 2G and 2H). In contrast, gene set analysis suggested that ribosomal subunit genes were broadly downregulated (Figures 2H, 2I, S2G, and S2H, Table S1).

Ribosomal subunit synthesis is under the control of mammalian target of rapamycin (mTOR) signaling (Mayer and Grummt, 2006), leading us to consider whether mTOR signaling might be reduced in muscle from BATI4KO mice. In support of this idea, TORC1 (raptor) ablation in skeletal muscle causes a form of muscular dystrophy with features reminiscent of BATI4KO mice, such as reduced oxidative capacity and centrally located nuclei (Bentzinger et al., 2008). Indeed, we found significantly reduced phosphorylation levels of the mTOR target p70S6K (T389) and a trend toward reduced mTOR phosphorylation (S2448) in the vastus of BATI4KO mice (Figure 2J).

Loss of IRF4 Induces a Myogenic Gene Expression Signature in BAT, Including the TGF-β Family Member Myostatin

Based on these data, we speculated that a myopathic factor was being secreted from the BAT of BATI4KO mice. We therefore performed RNA-seq on interscapular BAT from BATI4KO and control mice, which revealed 530 differentially regulated genes corresponding to $|\log_2 \text{fold change}| \geq 0.5$ and false discovery rate ≤ 0.25; of the 414 upregulated genes a huge number was related to myocyte differentiation and muscle function (Figures 3A, 3B, and S3A; Table S2). Interestingly, one of the upregulated genes was *Mstn*, encoding the secreted factor myostatin (Figures 3A and 3C), known to repress skeletal muscle hypertrophy in part via inhibition of mTOR signaling (Trendelenburg et al., 2009). Levels of Mstn protein were elevated in the BAT of BATI4KO mice, but not in muscle (Figures 3D and S3B–S3D). Importantly, myostatin was also elevated in the serum of BATI4KO mice (Figures 3E and S3E). Consistent with these data, levels of phospho-Smad3, a downstream effector of myostatin, were elevated in the vastus of BATI4KO mice (Figure S3F).

Brown Adipocytes from BATI4KO Mice Secrete Myostatin

We next assessed whether primary adipocytes from BATI4KO mice could be directly affecting muscle function via the secretion of myostatin, using a co-culture system (Figure 4A). We noted elevated expression of *Mstn* mRNA in isolated brown adipocytes from BATI4KO mice, accompanied by increased myostatin protein in the conditioned medium (Figures 4B and 4C). C2C12 myotubes cultured in contact with conditioned medium from BATI4KO adipocytes showed the same pattern of gene expression as the vastus muscle of BATI4KO mice *in vivo* (Figures 4D and 4E). They also showed reduced expression of mitochondrial proteins and reduced phosphorylation of mTOR on S2448, also similar to the phenotype of BATI4KO vastus *in vivo* (Figures 4F and 4G). Finally, isolated mitochondria from co-cultured myoblasts exhibited reduced ADP-stimulated and maximal OCR (Figure 4H).

Myostatin Mediates the Effect of BAT IRF4 Loss on Exercise Capacity

To test whether myostatin could be the myopathic factor affecting BATI4KO mice, we first employed a gain-of-function approach. A single injection of myostatin reduced exercise capacity in wild-type mice by 15%, and also induced a similar gene expression profile in the white vastus (Figures 5A, S4A, and S4B). We next employed two distinct loss-of-function strategies to assess the effect of blocking myostatin on exercise capacity in BATI4KO mice. In the first, we utilized single-dose administration of soluble activin receptor-Fc complex (sActRIIB-Fc) (Cadena et al., 2010), which successfully rescued running ability in BATI4KO mice (Figure 5B). There was no effect in control mice, and the effect washed out after 10 days, suggesting that the effect was not due to a hypertrophic effect on the muscles of treated mice. Because sActRIIB-Fc can bind other transforming growth factor β (TGF-β) family members in addition to myostatin, we next treated mice with a specific neutralizing anti-myostatin antibody (α-Mstn). A single injection of α-Mstn completely restored the ability of BATI4KO mice to run normally by 60 hr (Figure 5C). Gene expression patterns in vastus were also normalized by α-Mstn (Figure 5D). Again, re-testing mice 10 days after injection demonstrated that the effect is transient, and therefore not due to reprogramming or hypertrophy of muscle (Figure 5C). Levels of mTOR and p70S6k phosphorylation in vastus increased in BATI4KO mice treated with α-Mstn (Figure S4).

Mice Overexpressing IRF4 in BAT Run Better than Wild-Type Mice, and Have Reduced Serum Myostatin

We next tested whether overexpression of IRF4 in BAT (BATI4OE) could improve running ability in mice. BATI4OE mice show enhanced thermogenesis, and are lean and insulin sensitive on a high-fat diet (Kong et al., 2014). On chow diet, these mice show no differences in glucose or insulin tolerance testing, but they do exhibit higher exercise capacity by 24% (Figures 6A, S5A, and S5B). No clear morphological differences were noted in the vastus lateralis of these animals relative to controls by either light or electron microscopy (Figures S5C–S5G). However, ADP-stimulated and maximal mitochondrial respiration rates were increased in BATI4OE mice, as was mtDNA content (Figures 6B and 6C) in vastus lateralis, but not soleus

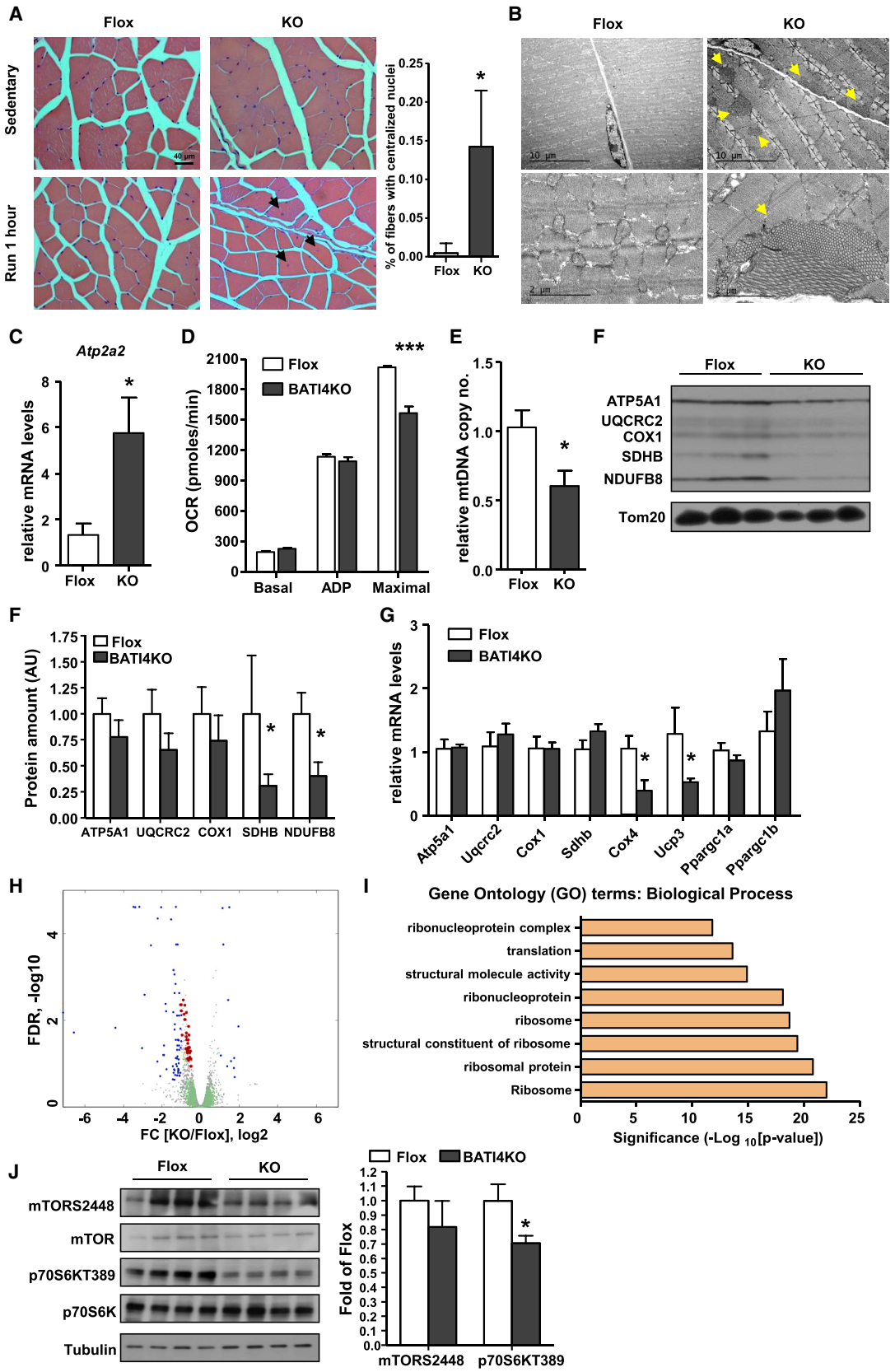

(legend on next page)

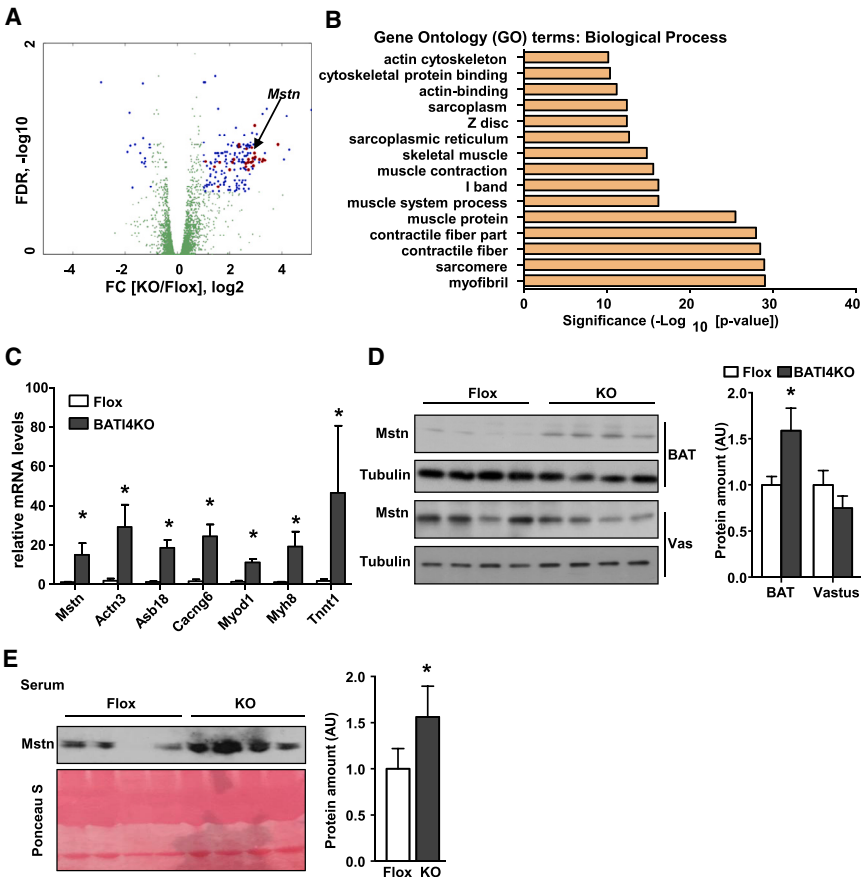

Figure 3. Loss of IRF4 Induces a Myogenic Gene Expression Signature in BAT, Including the TGF-β Family Member Myostatin

(A) Volcano plot of BAT RNA-seq. Blue and red dots represent significantly different genes between BATI4KO and Flox groups. Red dots represent muscle-related transcripts.

(B) GO analysis (biological process) of significantly different genes from RNA-seq analysis.

(C) qPCR analysis of selected muscle-related genes in BAT of male BATI4KO versus control mice (n = 5–6, *p < 0.05).

(D and E) Tissue (D) and serum (E) myostatin levels in BATI4KO versus control mice. Protein amount was quantified using Image J (n = 4, *p < 0.05 versus Flox mice).

All results are expressed as means ± SEM.

(Figure S5H). Furthermore, serum myostatin levels were decreased in BATI4OE mice (Figures 6D and S5I), and levels of *Mstn* mRNA and protein were decreased in the BAT, but not the muscle, of BATI4OE mice (Figures 6E, S5J, and S5K). Consistent with this, mTOR signaling in vastus from BATI4OE mice was enhanced relative to littermate controls (Figure 6F).

Thermoneutrality Induces Expression of Myostatin in BAT and Reduces Exercise Capacity

To put these findings into physiological context, we placed wild-type mice at thermoneutrality (30°C), a condition that profoundly reduces *Irf4* expression (Figure S6A). As predicted, warming resulted in a phenotype that is remarkably similar to BATI4KO; these mice show reduced exercise capacity by 14.5%, associated with elevated tissue and serum myostatin concentrations (Figures 7A–7C, S6B, and S6C). They also exhibit diminished mitochondrial protein expression and mTOR signaling in white vastus (Figures S6D and S6E). In addition, exposure to thermoneutrality induces a gene expression profile in vastus that is remarkably similar to that of BATI4KO mice (Figures S6F and S6G). To prove that thermoneutrality exerts these effects via BAT, we surgically removed interscapular BAT (iBATx) immediately prior to placement at 30°C. After 1 week of recovery (Figure S6H), iBATx mice showed improved exercise capacity relative to sham-operated controls, with decreased myostatin levels in serum (Figures 7D and 7E). Vastus mitochondrial protein levels, mTOR signaling, and mitochondrial and ribosomal gene expression were all normalized in iBATx mice relative to sham-operated controls (Figures 7F and S6I–S6K).

Figure 2. BATI4KO Mice Exhibit Myopathy

(A) H&E staining of vastus lateralis of BATI4KO and control mice (×40). Black arrows indicate nuclei that have migrated to the center of the myofiber after 1 hr of running. The percentage of myofibers with centralized nuclei was determined by manual counting (100–150 myofibers from 4 mice per group, *p < 0.05 versus Flox mice).

(B) Tubular aggregates (yellow arrows) in the vastus lateralis of male BATI4KO mice.

(C) *Atp2a2* expression in the vastus lateralis of male BATI4KO and control mice (n = 5–6, *p < 0.05 versus Flox).

(D) Measurement of oxygen consumption rate (OCR) in isolated mitochondria from vastus of male BATI4KO and control mice in the sedentary state (n = 7 mice per group, ***p < 0.0001 versus Flox mice).

(E) mtDNA content in the vastus lateralis of male BATI4KO and control mice (n = 4–5, *p < 0.05 versus Flox mice).

(F) Western blot analysis of isolated muscle mitochondria from BATI4KO and control mice. Protein amount was quantified using Image J (n = 3, *p < 0.05 versus Flox mice).

(G) qPCR analysis of mitochondrial gene expression in the vastus of male BATI4KO and control mice (n = 8–10, *p < 0.05 versus Flox).

(H) Volcano plot of vastus RNA-seq. Blue and red dots are significantly different between BATI4KO and Flox mice; red dots represent ribosomal subunit genes.

(I) Gene ontology (GO) analysis (biological process) of significantly different genes from RNA-seq analysis.

(J) Western blot analysis of mTOR signaling in vastus of male BATI4KO versus control mice. Activity was quantified using Image J (n = 4, *p < 0.05 versus Flox mice).

All results are expressed as means ± SEM.

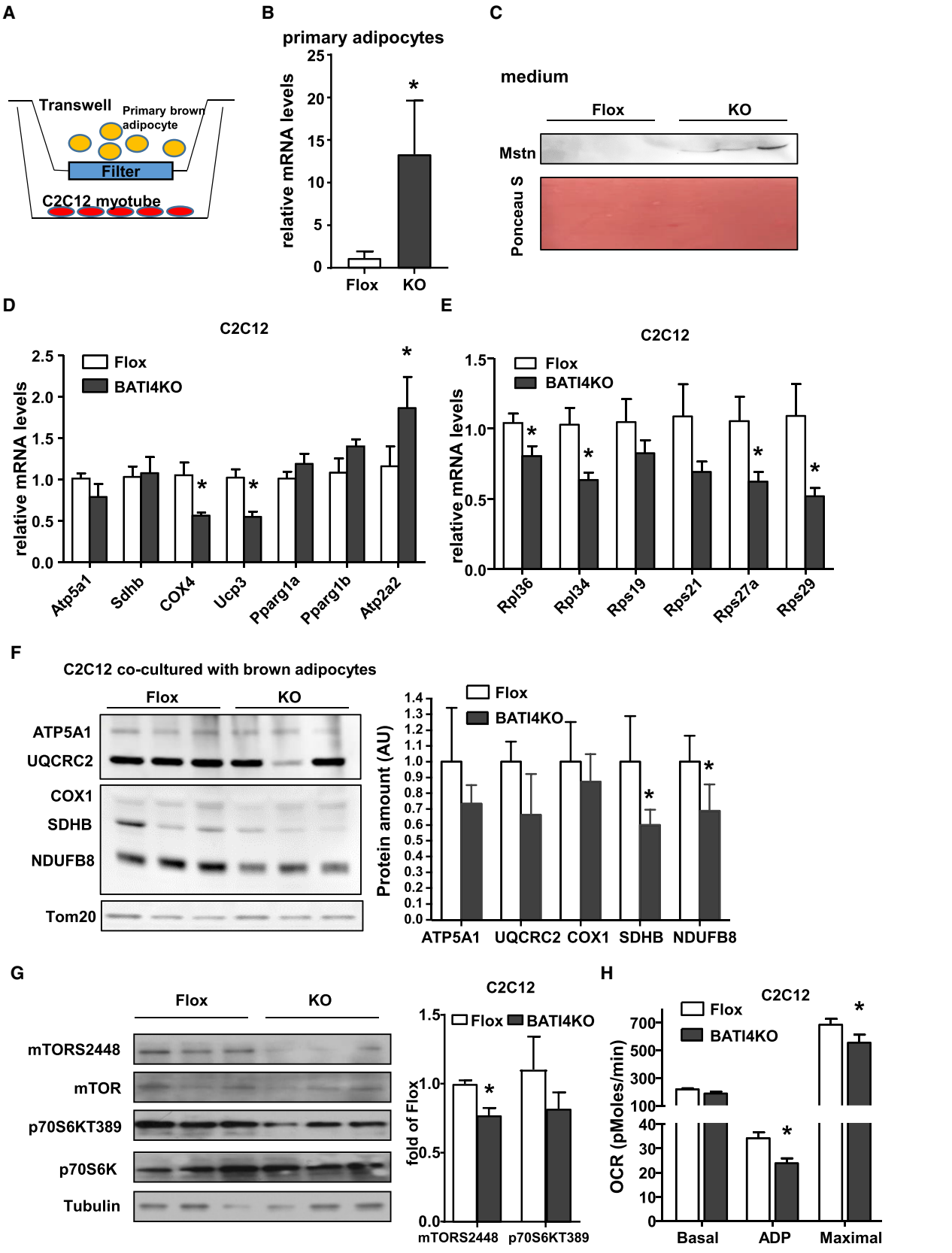

(legend on next page)

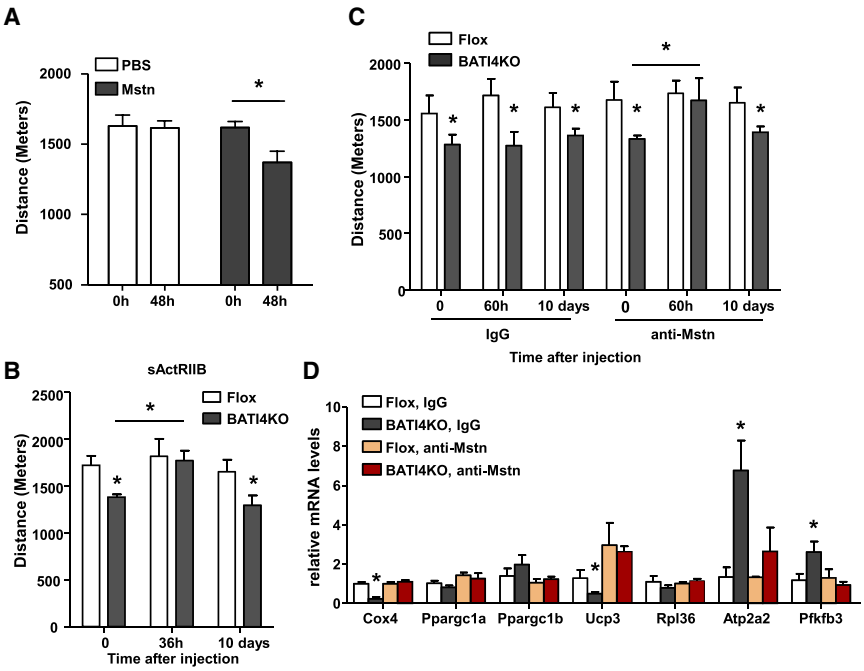

Figure 5. Myostatin Mediates the Effect of BAT IRF4 Loss on Exercise Capacity

(A) Low-intensity exercise regimen was performed in mice following a single injection of myostatin (n = 12–16, *p < 0.05 versus PBS).

(B) Exercise capacity determined in BATI4KO and control littermates before, 36 hr or 10 days following intraperitoneal injection of soluble ActRIIB (sActRIIB) with 10 mg/kg per mouse (n = 6–7, *p < 0.05 versus Flox mice).

(C) Exercise capacity was measured in BATI4KO and control littermates before, 60 hr or 10 days following a single intraperitoneal injection of myostatin-neutralizing antibodies or isotype control (n = 6–7, *p < 0.05 versus Flox mice).

(D) qPCR analysis of gene expression in vastus lateralis from sedentary mice treated as in (C), but samples were harvested before and 60 hr after injection (n = 5, *p < 0.05 versus Flox mice).

All results are expressed as means ± SEM.

DISCUSSION

BAT has long been thought to have one major function—generation of heat, which occurs when the mitochondrial proton gradient is dissipated by UCP1. This simplistic notion was challenged by the observation that ablation of BAT causes more profound metabolic consequences than knocking out UCP1 (Enerback et al., 1997; Lowell et al., 1993), leading to the proposition that BAT does something beyond heat generation. This idea was bolstered by the discovery of adipokines, secreted products of adipocytes that coordinate various aspects of energy homeostasis and metabolic physiology (Rosen and Spiegelman, 2014). In addition to a panoply of adipokines that are shared with white adipocytes, brown adipocytes secrete some factors that are unique to thermogenic cells. One example is neuregulin 4, an epidermal growth factor-like protein secreted by BAT that represses hepatic lipogenesis (Wang et al., 2014). Our discovery of a BAT-muscle axis that regulates exercise capacity is therefore in line with this burgeoning sense of what thermogenic adipocytes are, and what they can do.

A little more than a decade ago, similarities were noted in the transcriptional profiles of skeletal muscle and brown adipose precursor cells (Timmons et al., 2007). Additional studies using lineage-tracing techniques suggested that there might be a common Engrailed+ precursor that gives rise to both skeletal muscle and brown fat from a common central dermomyotome (Atit et al., 2006). Finally, brown adipocytes and skeletal muscle were shown to share a common Pax7$^+$, Myf5$^+$ lineage, and the transcription factors Ebf2, Pparγ, and Prdm16 were identified as key determinants favoring adipogenesis over myogenesis (Rajakumari et al., 2013; Seale et al., 2008). Our data suggest that Irf4 may play an important role in this process as well. Of note, loss of Irf4 in BAT does not cause a full reprogramming to muscle; Irf4 null brown adipocytes look like wild-type cells at the light-microscopic and ultrastructural level (Kong et al., 2014). They also continue to express most of the genes of wild-type brown adipocytes, albeit with some (e.g., *Ucp1* or *Ppargc1a*) at reduced levels (Kong et al., 2014). Instead, there is the appearance of a broad myogenic signature at low overall levels that probably results from actions at a few critical myogenic drivers, such as MyoD1. Presumably, the full muscle phenotype is not elaborated because the key repressors of their expression, such as Ebf2, Pparγ, and Prdm16, are still present.

Our BATI4KO data bring to mind recent work by the Brüning group, who found that optogenetic and chemogenetic activation of hypothalamic Agrp$^+$ neurons can promote the expression of a myogenic signature in BAT almost exactly the same as we show here (Steculorum et al., 2016). This makes sense, as activation of Agrp$^+$ neurons causes a sharp reduction in sympathetic activation of BAT (Krashes et al., 2011), which

Figure 4. Brown Adipocytes from BATI4KO Mice Secrete Myostatin

(A) Schematic illustration of co-culture.

(B) Elevated Mstn mRNA in primary brown adipocytes from BATI4KO mice (n = 5–6, *p < 0.05).

(C) Western blot analysis of co-culture medium myostatin levels. Protein amount was quantified using Image J (n = 3).

(D, E, and H) qPCR (D and E) and OCR (H) analysis of C_2C_{12} myotubes, co-cultured with BAT primary adipocyte from BATI4KO or control mice for 6 hr (*p < 0.05 versus Flox).

(F) Western blot analysis of mitochondria protein from co-cultured C_2C_{12} myotubes. Protein amount was quantified using Image J (n = 3, *p < 0.05 versus Flox).

(G) Western blot analysis of mTOR signaling pathway in co-cultured C_2C_{12} myotubes. Activity was quantified using Image J (n = 3, *p < 0.05 versus Flox).

All results are expressed as means ± SEM.

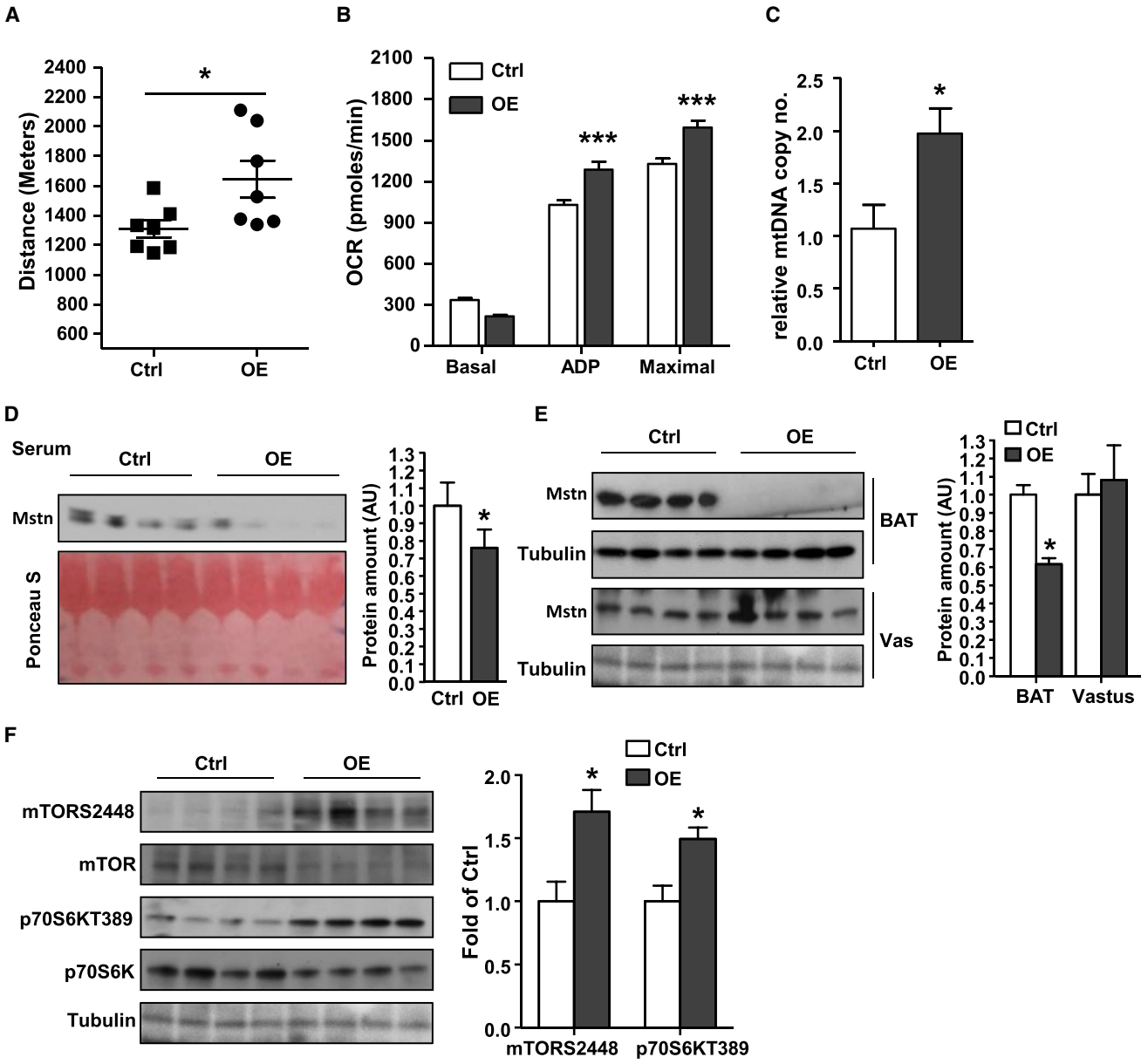

Figure 6. Mice Overexpressing IRF4 in BAT Run Better than Wild-Type Mice, and Have Reduced Serum Myostatin

(A) Exercise capacity in male BATI4OE mice (n = 7, *p < 0.05 versus control mice).

(B) Continuous measurement of OCR in isolated mitochondria from vastus of BATI4OE and control mice in the sedentary state (n = 6, ***p < 0.0001 versus control mice).

(C) mtDNA content in the vastus of male BATI4OE and control mice (n = 4–5, *p < 0.05 versus control mice).

(D and E) Serum and tissue myostatin level in BATI4OE versus control mice. Protein amount was quantified using Image J (n = 4, *p < 0.05 versus control mice).

(F) Western blot analysis of mTOR signaling pathway in vastus lateralis of BATI4OE and control mice. Activity was quantified using Image J (n = 4, *p < 0.05 versus control mice).

All results are expressed as means ± SEM.

would be expected to cause a decrease in IRF4 levels in BAT (Kong et al., 2014), akin to the effect that we see following thermoneutrality. Interestingly, Brüning and colleagues also identified myostatin secretion from BAT, which they showed acts in an autocrine manner to reduce local insulin sensitivity; no effect on muscle insulin sensitivity was noted during a hyperinsulinemic-euglycemic clamp.

The effects of myostatin on muscle have been studied extensively using either massive overexpression or complete knockout manipulations, which cause significant atrophy or hypertrophy, respectively (Allen et al., 2011; Dschietzig, 2014). In contrast, in our models we see neither atrophy nor hypertrophy. We speculate that this is because the changes in serum myostatin are relatively modest compared with these prolonged

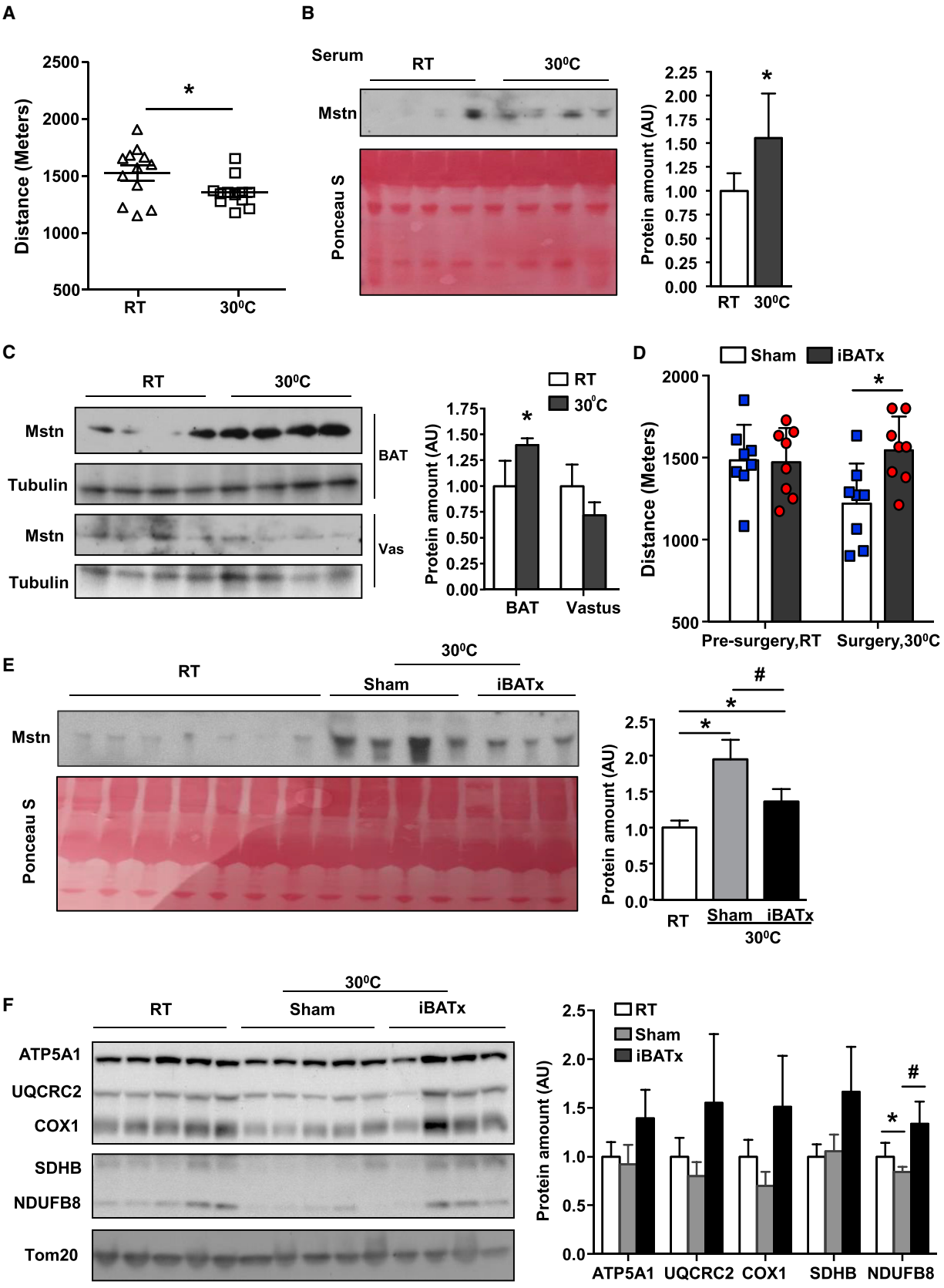

(legend on next page)

exposures to pharmacological levels, or complete absence of, myostatin. We also speculate that this may explain why some muscles, such as white vastus, are selectively affected.

Myostatin knockout mice have reduced body fat and improved metabolic phenotypes, and several studies have suggested direct effects on adipose tissue, including BAT. For example, thermogenic gene expression in myostatin null embryonic fibroblasts is repressed by the addition of exogenous myostatin (Braga et al., 2013). The acute inhibition of myostatin signaling using an inhibitor of ActRIIB causes increased BAT weight and improved mitochondrial function, energy expenditure, and cold tolerance (Fournier et al., 2012); however, soluble ActRIIB (as also used in our study) did not cause reduced fat mass in obese mice (McPherron et al., 2012).

Myostatin is believed to be produced primarily by muscle, and certainly the total amount of muscle in a mouse vastly exceeds the mass of BAT. Nevertheless, our data suggest that BAT contributes significantly to serum myostatin levels. In the BATI4KO model, we see elevated serum myostatin that corresponds to increased myostatin mRNA and protein in BAT, but not muscle. Conversely, our analysis of the BATI4OE model shows reduction of myostatin in BAT and serum, but not muscle. Finally, at thermoneutrality, we see a rise in serum myostatin by western blotting and ELISA that is largely reversed by BATectomy. The residual increment that remains after excision of BAT may be due to the small pockets of subscapular BAT that are not removed in the operation. Taken together, these data provide significant evidence that a component of murine serum myostatin derives from BAT, at least under certain environmental and genetic conditions. What portion of human serum myostatin derives from BAT, and under what conditions that may rise or fall, is unknown.

Is myostatin likely to be the only myopathic factor secreted by BAT at thermoneutrality, or in the presence of an IRF4 mutation? We show that a single dose of purified myostatin can cause the exercise phenotype. The studies in which myostatin is depleted by the soluble sActRIIB-Fc complex leading to complete restoration of exercise capacity leave open the possibility that related TGF-β family members, some of which can bind ActRIIB, may participate in the process. We did not see increased levels of such candidate factors in the IRF4 null BAT, but such a putative factor might not be regulated at the transcriptional level. The studies using a more specific antibody generated by Acceleron would seem to close that loophole. We therefore conclude that myostatin is likely to be a dominant, if perhaps not the only, player in this axis.

Tubular aggregates were first described in the 1960s in human muscle biopsies from certain patients with weakness and myalgia (Funk et al., 2013; Schiaffino, 2012). Although there was some early speculation that they may represent deformed mitochondria, it is now well established that they derive from SR. They are seen preferentially in type II muscle (especially type IIb fibers, which comprise 95% of the white vastus in mice) and in males. There is a cluster of rare familial tubular aggregate myopathies in humans caused by mutations in the genes *STIM1* and *ORAI1*, among others yet to be identified (Bohm et al., 2013; Endo et al., 2015); these genes were not changed at the mRNA level in muscles from BATI4KO mice (not shown). In mice, tubular aggregates can arise in several pathological situations, including uremia and aging (Funk et al., 2013; Schiaffino, 2012). Of note, wild-type C57Bl/6 mice do not show evidence of tubular aggregate formation in vastus until they reach 14 months of age (Agbulut et al., 2000); our BATI4KO mice, which are on a C57Bl/6 background, were only 10 weeks of age when tested. There is only a single reference in the literature that we are aware of connecting myostatin to tubular aggregates. In that study, constitutive global knockout of myostatin was associated with increased muscle mass, in particular an increased number of type IIb fibers, but with paradoxically reduced muscle force; tubular aggregate formation was noted in those fibers as well (Amthor et al., 2007). It is unclear how to put these results into context with our observations. Most likely tubular aggregate formation is simply a generic response to certain types of stress in murine type IIb fibers.

To our knowledge, the effect of thermal stress on exercise has not been systematically studied in animal models, although there are reports suggesting that pre-warming has detrimental effects on exercise capacity in humans (Gregson et al., 2005; Levels et al., 2014). We speculate that an organism might want to reduce the chance of hyperthermia by restricting exercise efficiency at high temperatures; in such a paradigm brown fat might be an ideal effector as an organ responsible for integrating thermal signals. Intriguingly, there are data showing that cold exposure can be used as a "cross-training" modality in sparrows, such that cold-exposed birds show enhanced muscle function and exercise performance; this is also associated with reduced serum myostatin (Zhang et al., 2015).

We have ascribed the exercise defect in BATI4KO mice to the pathology seen in white vastus, and possibly other muscles. It is worth noting that myostatin can also affect the heart, and this could contribute to the exercise phenotype. Myostatin is produced locally in heart muscle (Sharma et al., 1999), and levels rise in patients with heart failure (George et al., 2010). Surprisingly, germline deletion of myostatin does not lead to cardiac hypertrophy, although very old mice (28–30 months) were reported to have an increased normalized heart mass (Cohn et al., 2007; Mendias et al., 2015). Doxorubicin causes approximately equal

Figure 7. Thermoneutrality Induces Expression of Myostatin in BAT and Reduces Exercise Capacity

(A) Exercise capacity was measured in male wild-type C57Bl/6J mice after exposure to 30°C for 7 days (n = 10–12, *p < 0.05 versus RT).

(B and C) Serum (B) and BAT and vastus (C) levels of myostatin in mice housed at thermoneutrality versus RT. Protein amount was quantified using Image J (n = 4, *p < 0.05 versus RT).

(D) Exercise capacity in male iBATx mice (n = 8, *p < 0.05 versus sham).

(E) Serum myostatin level in mice before and after iBATx and exposure to 30°C. Protein amount was quantified using Image J (n = 3–7, *p < 0.05 versus RT; #p < 0.05 versus iBATx).

(F) Western blot analysis of isolated muscle mitochondria from mice before and after iBATx and exposure to 30°C. Protein amount was quantified using Image J (n = 4–5, *p < 0.05 versus RT; #p < 0.05 versus iBATx).

All results are expressed as means ± SEM.

wasting of cardiac and skeletal muscle; the effect on skeletal muscle can be largely prevented by administration of a myostatin receptor antagonist, while the heart toxicity was not affected (Hulmi et al., 2018). Taken together, these data suggest that cardiac muscle is likely to play a relatively minor role in the exercise phenotype seen in BATI4KO mice.

Finally, our models also resemble the situation in obesity, a condition with reduced functional BAT (van Marken Lichtenbelt et al., 2009), reduced IRF4 in BAT (Kong et al., 2014), elevated serum myostatin (Allen et al., 2011), and diminished ribosomal protein expression in skeletal muscle (Campbell et al., 2016). Conversely, bariatric surgery increases BAT activity (Vijgen et al., 2012), while also reducing serum myostatin (Park et al., 2006) and restoring ribosomal gene expression in muscle (Campbell et al., 2016).

In summary, we report here that BAT can secrete significant quantities of myostatin into the blood in response to warming, a situation that is mimicked by deleting IRF4 in BAT. In both of these situations, myostatin causes reduced mTOR signaling in type IIB muscle fibers, with a subsequent negative effect on translation. This seems to affect certain proteins preferentially, among them components of the mitochondrial electron transport chain. This in turn causes a bioenergetic defect in susceptible muscle, and a functional myopathy.

Taken together, our data provide evidence of an unsuspected level of inter-organ crosstalk between BAT and skeletal muscle, involving the transcription factor IRF4 and the secreted protein myostatin.

Limitations of Study

Our studies have a few limitations. First, although our data indicate that BAT contributes a non-negligible amount of myostatin to the serum, we are unable to fully quantify the extent of this contribution without tissue-specific ablation studies. Those studies are ongoing. We also cannot rule out the possibility that other BAT-derived factors may be affecting the phenotype. Such factors might work directly on skeletal muscle or may have indirect effects on exercise, such as through the availability or processing of liver glycogen. Consistent with this, we note that reduction of serum myostatin by either the soluble receptor or the neutralizing antibody improves exercise capacity in BATI4KO but not in floxed control mice. It is possible that BATI4KO mice have increased myostatin levels as well as increased sensitivity to myostatin. Finally, with respect to the quantitation of serum myostatin, we recognize that our western blot and ELISA data are concordant in direction, but not in magnitude. The reason for this is not clear to us, but may reflect higher nonspecific background in the ELISA system.

STAR★METHODS

Detailed methods are provided in the online version of this paper and include the following:

SUPPLEMENTAL INFORMATION

Supplemental Information includes six figures and three tables and can be found with this article online at https://doi.org/10.1016/j.cmet.2018.07.004.

ACKNOWLEDGMENTS

The authors gratefully acknowledge the Electron Microscopy core of the BIDMC. John Shelton in the Molecular Pathology Core in the Division of Cardiology at UT Southwestern performed the ATPase staining. Scott Pearsall at Acceleron provided myostatin, Mstn neutralizing antibody, and the soluble ActRIIB receptor. We thank members of the Rosen and Spiegelman laboratories for helpful discussions and technical advice. This work was funded by R00 DK106550 to X.K., the Major Research Plan of the National Natural Science Foundation of China (91749104), the Shanghai Pujiang Talent Project (18PJ1400700), the Science and Technology Innovation Action Plan of Shanghai Science and Technology Committee (18140901300), the Open Research Fund of the State Key Laboratory of Pharmaceutical Biotechnology (KF-GN-201701) to T.L., NIH R01 DK31405 to B.M.S., NIH R37 DK43051 to B.B.K., and NIH R01 DK085171, DK102173, DK113669, and DK102170 to E.D.R.

AUTHOR CONTRIBUTIONS

The experimental plan was designed by X.K., T.L., and E.D.R. X.K., T.L., T.Y., P.Z., and L.K. performed the experiments and analyzed the data. D.T. generated RNA-seq data, which was analyzed by A.L., B.A.D., and L.T. X.K. and E.D.R. wrote the manuscript, incorporating edits and comments from B.B.K., B.M.S, and all other authors. E.D.R. is the senior and corresponding author.

DECLARATION OF INTERESTS

E.D.R. is a paid consultant of Novartis. B.B.K. consults for Ironwood Pharmaceuticals and Alterna and serves on the Scientific Advisory Board of Janssen Pharmaceuticals. B.M.S. consults for Calico.

Received: February 6, 2018
Revised: May 11, 2018
Accepted: July 6, 2018
Published: August 2, 2018

REFERENCES

Agbulut, O., Destombes, J., Thiesson, D., and Butler-Browne, G. (2000). Age-related appearance of tubular aggregates in the skeletal muscle of almost all male inbred mice. Histochem. Cell Biol. *114*, 477–481.

Allen, D.L., Hittel, D.S., and McPherron, A.C. (2011). Expression and function of myostatin in obesity, diabetes, and exercise adaptation. Med. Sci. Sports Exerc. *43*, 1828–1835.

Amthor, H., Macharia, R., Navarrete, R., Schuelke, M., Brown, S.C., Otto, A., Voit, T., Muntoni, F., Vrbova, G., Partridge, T., et al. (2007). Lack of myostatin

results in excessive muscle growth but impaired force generation. Proc. Natl. Acad. Sci. USA *104*, 1835–1840.

Atit, R., Sgaier, S.K., Mohamed, O.A., Taketo, M.M., Dufort, D., Joyner, A.L., Niswander, L., and Conlon, R.A. (2006). Beta-catenin activation is necessary and sufficient to specify the dorsal dermal fate in the mouse. Dev. Biol. *296*, 164–176.

Bentzinger, C.F., Romanino, K., Cloetta, D., Lin, S., Mascarenhas, J.B., Oliveri, F., Xia, J., Casanova, E., Costa, C.F., Brink, M., et al. (2008). Skeletal muscle-specific ablation of raptor, but not of rictor, causes metabolic changes and results in muscle dystrophy. Cell Metab. *8*, 411–424.

Bohm, J., Chevessier, F., Maues De Paula, A., Koch, C., Attarian, S., Feger, C., Hantai, D., Laforet, P., Ghorab, K., Vallat, J.M., et al. (2013). Constitutive activation of the calcium sensor STIM1 causes tubular-aggregate myopathy. Am. J. Hum. Genet. *92*, 271–278.

Bostrom, P., Wu, J., Jedrychowski, M.P., Korde, A., Ye, L., Lo, J.C., Rasbach, K.A., Bostrom, E.A., Choi, J.H., Long, J.Z., et al. (2012). A PGC1-alpha-dependent myokine that drives brown-fat-like development of white fat and thermogenesis. Nature *481*, 463–468.

Braga, M., Pervin, S., Norris, K., Bhasin, S., and Singh, R. (2013). Inhibition of in vitro and in vivo brown fat differentiation program by myostatin. Obesity (Silver Spring) *21*, 1180–1188.

Cadena, S.M., Tomkinson, K.N., Monnell, T.E., Spaits, M.S., Kumar, R., Underwood, K.W., Pearsall, R.S., and Lachey, J.L. (2010). Administration of a soluble activin type IIB receptor promotes skeletal muscle growth independent of fiber type. J. Appl. Physiol. (1985) *109*, 635–642.

Campbell, L.E., Langlais, P.R., Day, S.E., Coletta, R.L., Benjamin, T.R., De Filippis, E.A., Madura, J.A., 2nd, Mandarino, L.J., Roust, L.R., and Coletta, D.K. (2016). Identification of novel changes in human skeletal muscle proteome after roux-en-Y gastric bypass surgery. Diabetes *65*, 2724–2731.

Cohen, P., Levy, J.D., Zhang, Y., Frontini, A., Kolodin, D.P., Svensson, K.J., Lo, J.C., Zeng, X., Ye, L., Khandekar, M.J., et al. (2014). Ablation of PRDM16 and beige adipose causes metabolic dysfunction and a subcutaneous to visceral fat switch. Cell *156*, 304–316.

Cohn, R.D., Liang, H.Y., Shetty, R., Abraham, T., and Wagner, K.R. (2007). Myostatin does not regulate cardiac hypertrophy or fibrosis. Neuromuscul. Disord. *17*, 290–296.

DeBalsi, K.L., Wong, K.E., Koves, T.R., Slentz, D.H., Seiler, S.E., Wittmann, A.H., Ilkayeva, O.R., Stevens, R.D., Perry, C.G., Lark, D.S., et al. (2014). Targeted metabolomics connects thioredoxin-interacting protein (TXNIP) to mitochondrial fuel selection and regulation of specific oxidoreductase enzymes in skeletal muscle. J. Biol. Chem. *289*, 8106–8120.

Dschietzig, T.B. (2014). Myostatin - from the Mighty Mouse to cardiovascular disease and cachexia. Clin. Chim. Acta *433*, 216–224.

Eguchi, J., Wang, X., Yu, S., Kershaw, E.E., Chiu, P.C., Dushay, J., Estall, J.L., Klein, U., Maratos-Flier, E., and Rosen, E.D. (2011). Transcriptional control of adipose lipid handling by IRF4. Cell Metab. *13*, 249–259.

Eguchi, J., Yan, Q.W., Schones, D.E., Kamal, M., Hsu, C.H., Zhang, M.Q., Crawford, G.E., and Rosen, E.D. (2008). Interferon regulatory factors are transcriptional regulators of adipogenesis. Cell Metab. *7*, 86–94.

Endo, Y., Noguchi, S., Hara, Y., Hayashi, Y.K., Motomura, K., Miyatake, S., Murakami, N., Tanaka, S., Yamashita, S., Kizu, R., et al. (2015). Dominant mutations in ORAI1 cause tubular aggregate myopathy with hypocalcemia via constitutive activation of store-operated Ca(2)(+) channels. Hum. Mol. Genet. *24*, 637–648.

Enerback, S., Jacobsson, A., Simpson, E.M., Guerra, C., Yamashita, H., Harper, M.E., and Kozak, L.P. (1997). Mice lacking mitochondrial uncoupling protein are cold-sensitive but not obese. Nature *387*, 90–94.

Falcon, S., and Gentleman, R. (2007). Using GOstats to test gene lists for GO term association. Bioinformatics *23*, 257–258.

Fournier, B., Murray, B., Gutzwiller, S., Marcaletti, S., Marcellin, D., Bergling, S., Brachat, S., Persohn, E., Pierrel, E., Bombard, F., et al. (2012). Blockade of the activin receptor IIb activates functional brown adipogenesis and thermogenesis by inducing mitochondrial oxidative metabolism. Mol. Cell. Biol. *32*, 2871–2879.

Fresno, C., and Fernandez, E.A. (2013). RDAVIDWebService: a versatile R interface to DAVID. Bioinformatics *29*, 2810–2811.

Funk, F., Ceuterick-de Groote, C., Martin, J.J., Meinhardt, A., Taratuto, A.L., De Bleecker, J., Van Coster, R., De Paepe, B., Schara, U., Vorgerd, M., et al. (2013). Morphological spectrum and clinical features of myopathies with tubular aggregates. Histol. Histopathol. *28*, 1041–1054.

George, I., Bish, L.T., Kamalakkannan, G., Petrilli, C.M., Oz, M.C., Naka, Y., Sweeney, H.L., and Maybaum, S. (2010). Myostatin activation in patients with advanced heart failure and after mechanical unloading. Eur. J. Heart Fail. *12*, 444–453.

Gregson, W.A., Batterham, A., Drust, B., and Cable, N.T. (2005). The influence of pre-warming on the physiological responses to prolonged intermittent exercise. J. Sports Sci. *23*, 455–464.

Hulmi, J.J., Nissinen, T.A., Rasanen, M., Degerman, J., Lautaoja, J.H., Hemanthakumar, K.A., Backman, J.T., Ritvos, O., Silvennoinen, M., and Kivela, R. (2018). Prevention of chemotherapy-induced cachexia by ACVR2B ligand blocking has different effects on heart and skeletal muscle. J. Cachexia Sarcopenia Muscle *9*, 417–432.

Ikeda, K., Kang, Q., Yoneshiro, T., Camporez, J.P., Maki, H., Homma, M., Shinoda, K., Chen, Y., Lu, X., Maretich, P., et al. (2017). UCP1-independent signaling involving SERCA2b-mediated calcium cycling regulates beige fat thermogenesis and systemic glucose homeostasis. Nat. Med. *23*, 1454–1465.

Kajimura, S., Spiegelman, B.M., and Seale, P. (2015). Brown and beige fat: physiological roles beyond heat generation. Cell Metab. *22*, 546–559.

Kazak, L., Chouchani, E.T., Jedrychowski, M.P., Erickson, B.K., Shinoda, K., Cohen, P., Vetrivelan, R., Lu, G.Z., Laznik-Bogoslavski, D., Hasenfuss, S.C., et al. (2015). A creatine-driven substrate cycle enhances energy expenditure and thermogenesis in beige fat. Cell *163*, 643–655.

Kazak, L., Chouchani, E.T., Lu, G.Z., Jedrychowski, M.P., Bare, C.J., Mina, A.I., Kumari, M., Zhang, S., Vuckovic, I., Laznik-Bogoslavski, D., et al. (2017). Genetic depletion of adipocyte creatine metabolism inhibits diet-induced Thermogenesis and drives obesity. Cell Metab. *26*, 693.

Kim, D., Pertea, G., Trapnell, C., Pimentel, H., Kelley, R., and Salzberg, S.L. (2013). TopHat2: accurate alignment of transcriptomes in the presence of insertions, deletions and gene fusions. Genome Biol. *14*, R36.

Kong, X., Banks, A., Liu, T., Kazak, L., Rao, R.R., Cohen, P., Wang, X., Yu, S., Lo, J.C., Tseng, Y.H., et al. (2014). IRF4 is a key thermogenic transcriptional partner of PGC-1alpha. Cell *158*, 69–83.

Kong, X., Wang, R., Xue, Y., Liu, X., Zhang, H., Chen, Y., Fang, F., and Chang, Y. (2010). Sirtuin 3, a new target of PGC-1alpha, plays an important role in the suppression of ROS and mitochondrial biogenesis. PLoS One *5*, e11707.

Krashes, M.J., Koda, S., Ye, C., Rogan, S.C., Adams, A.C., Cusher, D.S., Maratos-Flier, E., Roth, B.L., and Lowell, B.B. (2011). Rapid, reversible activation of AgRP neurons drives feeding behavior in mice. J. Clin. Invest. *121*, 1424–1428.

Levels, K., de Koning, J.J., Mol, E., Foster, C., and Daanen, H.A. (2014). The effect of pre-warming on performance during simulated firefighting exercise. Appl. Ergon. *45*, 1504–1509.

Liao, Y., Smyth, G.K., and Shi, W. (2014). featureCounts: an efficient general purpose program for assigning sequence reads to genomic features. Bioinformatics *30*, 923–930.

Lowell, B.B., S-Susulic, V., Hamann, A., Lawitts, J.A., Himms-Hagen, J., Boyer, B.B., Kozak, L.P., and Flier, J.S. (1993). Development of obesity in transgenic mice after genetic ablation of brown adipose tissue. Nature *366*, 740–742.

Mayer, C., and Grummt, I. (2006). Ribosome biogenesis and cell growth: mTOR coordinates transcription by all three classes of nuclear RNA polymerases. Oncogene *25*, 6384–6391.

McPherron, A.C., Guo, T., Wang, Q., and Portas, J. (2012). Soluble activin receptor type IIB treatment does not cause fat loss in mice with diet-induced obesity. Diabetes Obes. Metab. *14*, 279–282.

Mendias, C.L., Bakhurin, K.I., Gumucio, J.P., Shallal-Ayzin, M.V., Davis, C.S., and Faulkner, J.A. (2015). Haploinsufficiency of myostatin protects against

aging-related declines in muscle function and enhances the longevity of mice. Aging Cell *14*, 704–706.

Morgan-Hughes, J.A. (1998). Tubular aggregates in skeletal muscle: their functional significance and mechanisms of pathogenesis. Curr. Opin. Neurol. *11*, 439–442.

Park, J.J., Berggren, J.R., Hulver, M.W., Houmard, J.A., and Hoffman, E.P. (2006). GRB14, GPD1, and GDF8 as potential network collaborators in weight loss-induced improvements in insulin action in human skeletal muscle. Physiol. Genomics *27*, 114–121.

Rajakumari, S., Wu, J., Ishibashi, J., Lim, H.W., Giang, A.H., Won, K.J., Reed, R.R., and Seale, P. (2013). EBF2 determines and maintains brown adipocyte identity. Cell Metab. *17*, 562–574.

Rao, R.R., Long, J.Z., White, J.P., Svensson, K.J., Lou, J., Lokurkar, I., Jedrychowski, M.P., Ruas, J.L., Wrann, C.D., Lo, J.C., et al. (2014). Meteorin-like is a hormone that regulates immune-adipose interactions to increase beige fat thermogenesis. Cell *157*, 1279–1291.

Roberts, L.D., Bostrom, P., O'Sullivan, J.F., Schinzel, R.T., Lewis, G.D., Dejam, A., Lee, Y.K., Palma, M.J., Calhoun, S., Georgiadi, A., et al. (2014). beta-Aminoisobutyric acid induces browning of white fat and hepatic beta-oxidation and is inversely correlated with cardiometabolic risk factors. Cell Metab. *19*, 96–108.

Robinson, M.D., McCarthy, D.J., and Smyth, G.K. (2010). edgeR: a Bioconductor package for differential expression analysis of digital gene expression data. Bioinformatics *26*, 139–140.

Roman, W., and Gomes, E.R. (2017). Nuclear positioning in skeletal muscle. Semin. Cell Dev. Biol. https://doi.org/10.1016/j.semcdb.2017.11.005.

Rosen, E.D., and Spiegelman, B.M. (2014). What we talk about when we talk about fat. Cell *156*, 20–44.

Rothwell, N.J., and Stock, M.J. (1989). Surgical removal of brown fat results in rapid and complete compensation by other depots. Am. J. Physiol. *257*, R253–R258.

Schiaffino, S. (2012). Tubular aggregates in skeletal muscle: just a special type of protein aggregates? Neuromuscul. Disord. *22*, 199–207.

Schrauwen, P., and van Marken Lichtenbelt, W.D. (2016). Combatting type 2 diabetes by turning up the heat. Diabetologia *59*, 2269–2279.

Seale, P., Bjork, B., Yang, W., Kajimura, S., Chin, S., Kuang, S., Scime, A., Devarakonda, S., Conroe, H.M., Erdjument-Bromage, H., et al. (2008). PRDM16 controls a brown fat/skeletal muscle switch. Nature *454*, 961–967.

Sharma, M., Kambadur, R., Matthews, K.G., Somers, W.G., Devlin, G.P., Conaglen, J.V., Fowke, P.J., and Bass, J.J. (1999). Myostatin, a transforming growth factor-beta superfamily member, is expressed in heart muscle and is upregulated in cardiomyocytes after infarct. J. Cell. Physiol. *180*, 1–9.

Steculorum, S.M., Ruud, J., Karakasilioti, I., Backes, H., Engstrom Ruud, L., Timper, K., Hess, M.E., Tsaousidou, E., Mauer, J., Vogt, M.C., et al. (2016). AgRP neurons control systemic insulin sensitivity via myostatin expression in brown adipose tissue. Cell *165*, 125–138.

Timmons, J.A., Wennmalm, K., Larsson, O., Walden, T.B., Lassmann, T., Petrovic, N., Hamilton, D.L., Gimeno, R.E., Wahlestedt, C., Baar, K., et al. (2007). Myogenic gene expression signature establishes that brown and white adipocytes originate from distinct cell lineages. Proc. Natl. Acad. Sci. USA *104*, 4401–4406.

Trendelenburg, A.U., Meyer, A., Rohner, D., Boyle, J., Hatakeyama, S., and Glass, D.J. (2009). Myostatin reduces Akt/TORC1/p70S6K signaling, inhibiting myoblast differentiation and myotube size. Am. J. Physiol. Cell Physiol. *296*, C1258–C1270.

van Marken Lichtenbelt, W.D., Vanhommerig, J.W., Smulders, N.M., Drossaerts, J.M., Kemerink, G.J., Bouvy, N.D., Schrauwen, P., and Teule, G.J. (2009). Cold-activated brown adipose tissue in healthy men. N. Engl. J. Med. *360*, 1500–1508.

Vijgen, G.H., Bouvy, N.D., Teule, G.J., Brans, B., Hoeks, J., Schrauwen, P., and van Marken Lichtenbelt, W.D. (2012). Increase in brown adipose tissue activity after weight loss in morbidly obese subjects. J. Clin. Endocrinol. Metab. *97*, E1229–E1233.

Vosselman, M.J., van Marken Lichtenbelt, W.D., and Schrauwen, P. (2013). Energy dissipation in brown adipose tissue: from mice to men. Mol. Cell. Endocrinol. *379*, 43–50.

Wang, G.X., Zhao, X.Y., Meng, Z.X., Kern, M., Dietrich, A., Chen, Z., Cozacov, Z., Zhou, D., Okunade, A.L., Su, X., et al. (2014). The brown fat-enriched secreted factor Nrg4 preserves metabolic homeostasis through attenuation of hepatic lipogenesis. Nat. Med. *20*, 1436–1443.

Zhang, Y., Eyster, K., Liu, J.S., and Swanson, D.L. (2015). Cross-training in birds: cold and exercise training produce similar changes in maximal metabolic output, muscle masses and myostatin expression in house sparrows (*Passer domesticus*). J. Exp. Biol. *218*, 2190–2200.

STAR★METHODS

KEY RESOURCES TABLE

REAGENT or RESOURCE	SOURCE	IDENTIFIER
Antibodies		
Human/Mouse/Rat GDF-8/Myostatin Antibody	R&D Systems	RRID: AB_355600
Total OXPHOS Rodent WB Antibody Cocktail	Abcam	RRID: AB_2629281
Anti-Smad3 (phospho S423 + S425) antibody	Abcam	RRID: AB_882596
Phospho-mTOR (Ser2448) Antibody	Cell Signaling Technology	RRID: AB_330970
Phospho-p70 S6 Kinase (Thr389) (108D2) Rabbit mAb	Cell Signaling Technology	RRID: AB_2269803
mTOR Antibody	Cell Signaling Technology	RRID: AB_330978
p70 S6 Kinase (49D7) rabbit mAb	Cell Signaling Technology	RRID: AB_390722
α-Tubulin Antibody	Cell Signaling Technology	RRID: AB_10693793
Smad2/3 (D7G7) XP(R) Rabbit mAb	Cell Signaling Technology	RRID: AB_10889933
β-Actin Antibody	Cell Signaling Technology	RRID: AB_330288
Tom20 (FL-145)	Santa Cruz Biotechnology	RRID: AB_2207533
goat anti-rabbit IgG-HRP	Santa Cruz Biotechnology	RRID: AB_631747
donkey anti-goat IgG-HRP	Santa Cruz Biotechnology	RRID: AB_631728
goat anti-mouse IgG-HRP	Santa Cruz Biotechnology	RRID: AB_650499
Chemicals, Peptides, and Recombinant Proteins		
SYBR Green PCR Master Mix	Life Technologies	Cat# 4312704
Tragacanth	Sigma-Aldrich	g1128-100g
Rna Stat 60	Fisher Scientific	NC9256697
Recombinant Human/Mouse/Rat GDF-8/Myostatin Protein	R&D Systems	788-G8-010
Tissue-Tek O.C.T. Compound, Sakura Finetek	VWR	25608-930
Critical Commercial Assays		
GDF-8/Myostatin Quantikine ELISA Kit	R&D Systems	DGDF80
Express extract enzyme	Kapa Biosystems	KK7103
Readymix with dye	Kapa Biosystems	KK5621
Mitochondria Isolation Kit for Tissue (with Dounce Homogenizer)	Abcam	ab110169
NextSeq 500/550 High Output v2 Kit, 75 cycles	Illumina	FC-404-2005
DNeasy Blood & Tissue Kit	Qiagen	69506
Deposited Data		
RNA-seq	this study	GEO: GSE103736
Experimental Models: Cell Lines		
C2C12	ATCC	ATCC CRL-1772
Experimental Models: Organisms/Strains		
Mouse: C57BL/6J	Jackson Laboratory	RRID:IMSR_JAX:000664
Mouse: B6.FVB-Tg(Ucp1-cre)1Evdr/J	Jackson Laboratory	RRID:IMSR_JAX:024670
Mouse: B6;FVB-Tg(Adipoq-cre)1Evdr/J	Jackson Laboratory	RRID:IMSR_JAX:010803
Mouse: B6.129S1-Irf4tm1Rdf/J	Jackson Laboratory	RRID:IMSR_JAX:009380
Mouse: B6.129-Ucp1tm1Kz/J	Jackson Laboratory	RRID:IMSR_JAX:003124
Mouse: Rosa26-LSL-IRF4	PMID:24995979	N/A
Mouse: PRDM16 Floxed mice	PMID:24439384	N/A
Oligonucleotides		
A full list of Primers is in Table S3	This paper	N/A

(*Continued on next page*)

Continued

REAGENT or RESOURCE	SOURCE	IDENTIFIER
Software and Algorithms		
GraphPad Prism 7	GraphPad Software	https://www.graphpad.com/scientific-software/prism/
ImageJ Java 1.6.0_2.4	NIH	https://imagej.nih.gov/ij/

CONTACT FOR REAGENT AND RESOURCE SHARING

Further information and requests for resources and reagents should be directed to and will be fulfilled by the lead contact, Evan D. Rosen (erosen@bidmc.harvard.edu).

EXPERIMENTAL MODEL AND SUBJECT DETAILS

Animal Care

Mice were maintained under a 12 hr light/12hr dark cycle at constant temperature (23°C) with free access to food and water. BATI4KO, BATI4OE, and adipose-specific Prdm16 KO mice were generated as described (Cohen et al., 2014; Kong et al., 2014). All mice were extensively back-crossed onto a C57Bl/6J background. All animal studies were approved by the Institutional Animal Care and Use Committee of the Beth Israel Deaconess Medical Center and UCLA.

Thermoneutrality Stimulation

Male C57BL/6J mice housed at 30°C were fed chow diet with free access to water and food for a week. Mice were maintained under a 12 hr light/12 hr dark cycle. After one week, mice were measured exercise capacity compared with those housed at room temperature. At the end of the studies, all animals were euthanized by cervical dislocation, trunk blood was collected and centrifuged (800 g, 20 min) to generate plasma and BAT and muscle tissues were removed, frozen in liquid nitrogen and stored at −80°C for later analyses.

Surgical Removal of Interscapular BAT (iBATX)

To remove interscapular BAT, we used a modified procedure based on (Rothwell and Stock, 1989). Animals were anesthetized by intraperitoneal injection of 4% chloral hydrate (10 μL/g body weight: Sigma-c8383). A small longitudinal incision was made between the shoulder blades and the skin carefully opened. Sulzer's vein draining the iBAT was located and tied off above the point of branching into the two iBAT lobes. The vein was then cut on the iBAT side of the tie and the two iBAT lobes were quickly and completely removed. The incision was closed and animals were allowed to recover. Control mice were given the same dose of anesthesia, and had the skin opened and closed. All mice were treated with the pain-killer meloxicam (Zoopharm) before surgery. Mice were maintained under a 12 hr light/12 hr dark cycle at constant temperature (30°C) with free access to food and water and fed on a standard chow diet after surgery. Body weight was monitored every day until recovery.

Measurement of Exercise Capacity

All mice were acclimated to the treadmill 4-5 days prior to the exercise test session. Before each session, food was removed 2 hr before exercise. Acclimation began at a low speed of 5 to 8 meters per minute (m/min) for a total of 10 min on Day 1, and was increased to 5 to 10 m/min for a total of 10 min on Day 2. Following this, the mice were allowed to rest for at least 2 days in their home cage. For the low intensity treadmill test, the treadmill began at a rate of 12 m/min for 40 min. After 40 min, the treadmill speed was increased at a rate of 1 m/min every 10 min for a total of 30 min, and then increased at the rate of 1 m/min every 5 min until the mice were exhausted (mice spent more than 5 seconds on the electric shocker without resuming running). The high intensity treadmill test was conducted on an open field six-lane treadmill set at a 10% incline. Following a 5-min 0m/min acclimation period, the speed was raised to 6 m/min and increased by 2 m/min every 5 min to a maximal pace of 30 m/min until exhaustion (DeBalsi et al., 2014). Individual experiments were replicated 2-4 times.

Myostatin Tail Vein Injection

10-week-old male C57BL mice were injected with myostatin (1 μg/g BW) (Acceleron, Boston, MA, USA) or PBS through tail vein. 48 hr after injection, mice either underwent exercise capacity testing or were euthanized by cervical dislocation for sample collection; muscle tissues were removed, frozen in liquid nitrogen and stored at −80°C for later analyses. Individual experiments were replicated 2-4 times.

Anti-Myostatin Blockade and sActRIIB Injection

10- to 14-week-old male BATI4KO and control mice received intraperitoneal (IP) injections of anti-myostatin (antiGDF8) or control IgG, or recombinant soluble ActRIIB (10 mg/kg) (Acceleron, Boston, MA, USA) in sterile TBS (1.0 mg/mL) (n = 6-7). 60 hr

(for anti-myostatin and IgG groups)/ 36hours (sActRIIB group) after the injection, mice were either measured exercise capacity or euthanized by cervical dislocation, trunk blood was collected and centrifuged (800 g, 20 min) to generate plasma and BAT and muscle tissues were removed, frozen in liquid nitrogen and stored at −80°C for later analyses. Individual experiments were replicated 2-4 times.

Primary Adipocytes and Co-Culture

The interscapular brown fat pad was dissected from male mice (8-10 weeks), minced, and then digested for 45 min at 37°C in isolation buffer [PBS containing 10 mM $CaCl_2$, 2.4 U mL 21 dispase II (Roche) and 1.5 U mL 21 collagenase D (Roche)]. Digested tissue was filtered through a 100 um cell strainer to remove large pieces, and the flow-through was then centrifuged for 10 min at 600x g to collect the supernatant (mature adipocytes) and transfer to a new 15 mL tube. Wash the supernatant with 2 mL medium (DMEM/F12 (1:1; Invitrogen)), and then repeat the spinning and wash for 4 times. Suck the supernatant to the trans-well and co-cultured with differentiated C2C12 myotubes for 6 hr. Then the C2C12 cells were collected for indicated measurements.

METHOD DETAILS

Bioenergetics

Tissue respiration was performed using a Clark electrode (Strathkelvin Instruments). For mitochondrial bioenergetic analyses, vastus mitochondria were isolated in SHE buffer, pH 7.4 (250 mM sucrose, 5 mM Tris, pH 7.4, 1 mM EGTA) via differential centrifugation. Mitochondria were resuspended in respiration buffer (210 mM Mannitol, 70 mM Sucrose, 3 mM MgCl2, 5 mM KH2PO4, 20 mM Tris [pH 7.4], 0.1 mM EGTA, 0.1% BSA, 10 mM Pyruvate, 5 mM Malate). Oxygen consumption of vastus mitochondria (15 μg) was determined using an XF24e Extracellular Flux Analyzer (Seahorse Bioscience). ADP-stimulated respiration was triggered with 0.2 mM ADP. Maximal oxygen consumption was determined using FCCP (10 μM).

Mitochondrial DNA Copy Number

Mitochondrial DNA (mtDNA) copy number was determined as a marker for mitochondrial density using quantitative RT-PCR as previously reported(Kong et al., 2010). Briefly, total DNA was isolated from the cells using DNeasy Blood & Tissue Kit (Qiagen, 69506) according to the manufacturer's instructions. The mitochondrial DNA copy-number was calculated from the ratio of COX II (mitochondrial-encoded gene)/cyclophilin A (nuclear-encoded gene).

Histology

The vastus lateralis muscles of 12-week-old male mice were harvested. Muscles were preserved in 4% formaldehyde, bisected at the mid-belly and embedded in paraffin. 5-μm sections from muscle centers were stained with hematoxylin and eosin. The mean CSA of fibers ($n > 400$) in three fields from each animal ($n = 3$-6) was determined using the Image J program. H&E staining was performed using a standard protocol. The percentage of myofibers with centralized nuclei was determined by manual counting. The number of fibers exhibiting centralized (internal) nuclei was divided by the total number of fibers in the tissue cross-section (100–150) myofibers from 4 mice per group.

Picrosirius Red Staining was performed to detect fibrosis in muscle. We followed the manufacturer's instructions (Polysciences, #24901). Briefly, sections of muscle were deparaffinized and rehydrated in distilled water, followed by staining. Finally, samples were dehydrated, cleared, and mounted, followed by imaging using light microscopy.

RNA-seq Library Generation and Analysis

Five replicates (each one an individual mouse) were prepared, sequenced, and analyzed separately. mRNA was purified from 70 ng of total RNA using the Ribo-Zero Magnetic Gold Kit (Illumina, catalog# MRZG126). Libraries were prepared using the TruSeq RNA Library Preparation Kit v2 (Illumina, catalog #RS-122-2001) according to the manufacturer's protocol starting with the EPF step. Sequencing was performed on the Illumina HiSeq2500. RNA-seq data were aligned using TopHat2(Kim et al., 2013) to the mm9 mouse genome, and duplicates and low-quality reads were removed by Picard (http://picard.sourceforge.net). Reads were assigned to transcripts, normalized, and quantified using featureCounts (Liao et al., 2014) and EdgeR(Robinson et al., 2010). Low expressed genes (log2 CPM <1) were filtered out. Gene set enrichment analysis was performed using RDAVIDWebService (Fresno and Fernandez, 2013) and GOstats (Falcon and Gentleman, 2007).

QUANTIFICATION AND STATISTICAL ANALYSIS

Unpaired two-tailed Student's t test and two-way ANOVA were used. $p < 0.05$ was considered statistically significant.

DATA AND SOFTWARE AVAILABILITY

The accession number for the RNA-seq data reported in this paper is GEO: GSE103736. All bioinformatics software used in the study are publicly available; the volcano plotter we developed is publicly available (https://bdawes.shinyapps.io/volcano_plotter/).